

Article

Performance Analysis of Marine-Predator-Algorithm-Based Optimum PI Controller with Unified Power Flow Controller for Loss Reduction in Wind–Solar Integrated System

Chandu Valuva  and Subramani Chinnamuthu * 

Department of Electrical and Electronics Engineering, SRM Institute of Science and Technology, Kattankulathur 603203, India; chanduv43@gmail.com

* Correspondence: csmsrm@gmail.com; Tel.: +91-9600013988

Abstract: Transmission line losses are a crucial and essential issue in stable power system operation. Numerous methodologies and techniques prevail for minimizing losses. Subsequently, Flexible Alternating Current Transmission Systems (FACTSs) efficiently reduce transmission losses, and the Unified Power Flow Controller (UPFC) is a reactive power compensation controller. The parameter strength of the proportional–integral (PI) controller was calibrated with the Marine Predator Algorithm (MPA), a recent metaheuristic algorithm. An MPA-based optimum PI controller with a UPFC evaluates the optimal location of the UPFC and PI controller parameters to accomplish the desired research objective. The power rating of the UPFC was determined depending on the voltage collapse rating and power loss and an evaluated performance analysis of the MPA–PI-controlled UPFC on a modified IEEE-30 bus transmission network in MATLAB Simulink code. The Newton–Raphson method was used to perform the load flow analysis. Hence, the proposed MPA–PI controller was examined in contrast to preferred heuristic algorithms, the Artificial Bee Colony (ABC) and Moth Flame Optimization algorithms (MFO); the results showed that the MPA–PI controller exhibited better performance with an improved voltage profile and surpasses active power losses with the optimal placement of the UPFC device under different loading conditions. The active power loss, considering a UPFC with the proposed algorithm, reduced from 0.0622 p.u to 0.0301 p.u; consequently, the voltage profile was improved in the respective buses, and the loss percentage reduction during a 100% base load was 68.39%, which was comparatively better than the ABC and MFO algorithms.

Keywords: loss minimization; proportional–integral controller; FACTS; unified power flow controller; marine predator algorithm



Citation: Valuva, C.; Chinnamuthu, S. Performance Analysis of Marine-Predator-Algorithm-Based Optimum PI Controller with Unified Power Flow Controller for Loss Reduction in Wind–Solar Integrated System. *Energies* **2023**, *16*, 6157. <https://doi.org/10.3390/en16176157>

Academic Editors: Doug Arent, Xiaolei Yang and Adam Warren

Received: 26 July 2023

Revised: 14 August 2023

Accepted: 17 August 2023

Published: 24 August 2023



Copyright: © 2023 by the authors. Licensee MDPI, Basel, Switzerland. This article is an open access article distributed under the terms and conditions of the Creative Commons Attribution (CC BY) license (<https://creativecommons.org/licenses/by/4.0/>).

1. Introduction

Renewable energy sources rapidly evolve in power and energy production, and current demand significantly focuses on enhancing the utilization of renewable energy. There is a compulsion to supply the demand for global energy and to reduce global warming, the consequence of climate conditions, which are affected by the usage of fossil fuels for electrical power generation; hence, the power generation has to be constrained for sustainable and renewable energy generation. It has turned the worldwide researcher’s focus to renewable energy conversion in designing and developing an alternative to conventional fossil fuel energy. All over the world, advanced countries like India, China, Japan, North America, and Europe have been investing money in expanding renewable energy systems [1]. Renewable energies like wind and solar energies are dominant sustainable energy sources. The Global Wind Energy Council annual report of 2023 declared that 77.6 GW of wind power capacity was established in 2022. With comprehensive energy, it reached 906 GW of wind energy, a 9% growth compared to 2021. This year, it may reach 100 GW of new capacity installed globally with a growth of 15%. The intelligence market predicts

680 GW of new capacity within the next 5 years. That represents 136 GW of power per year from 2023 to 2027 [2].

The Marine Predator Algorithm (MPA) is a contemporary environment-energized optimization algorithm derived from outspread foraging strategies in ocean predators dependent on Levy and Brownian motions [3]. The MPA is a dynamic heuristic algorithm with numerous benefits, like a gradient-free nature, flexibility, fewer parameters, and an effortless mechanism. Predators must adopt a desirable strategy for maximizing their action levy with prey depending on the “survival of the fittest” theory. The MPA is a multi-objective optimization problem with a series of resolutions reproducing the finest swapping among the multiple objectives, usually in striving. Anyhow, the existence of multiple optimal solutions would assist the decision makers in determining the suitable result for their difficulty. A proportional–integral (PI) controller is a feedback control system type universally operated to standardize and strengthen systems in industrial and engineering applications. A PI controller is an essential element in control theory; moreover, it is employed for the systematic regulation of different equipment, systems, and processes. PI controllers are comparatively flexible to execute with an efficient performance in control theory. The proposed controller performance was analyzed considering different load conditions. The main intention of this article’s MPA-based optimum PI controller of a UPFC was to reduce the losses in wind–solar-integrated transmission systems. The MPA-based PI controller regulates the parameter input to the UPFC, which mitigates the voltage instability and reduces the active power losses; moreover, it enhances the system performance. The proposed MPA optimization algorithm tunes the parameters of the PI controller fed to the UPFC device. This article is about the analysis of the performance of a modified IEEE 30 system integrated with wind–solar with different load variations.

Various authors have investigated the potentialities, capabilities, and challenges of accomplishing 100% renewable energy generation. In [4], the authors insisted that 100% renewable energy is not attainable. Their analysis considered suitable research, constituting the distribution and transmission conditions and supplementary requirements to attain 100% renewable energy. Yet, certain defendants for 100% renewable energy have intensely explained the probability of attaining 100% renewable energy. The authors of [5] demonstrated in detail and with reliable reasoning against the data presented in [4] that 100% renewable energy is technically attainable and economically possible. Some researchers have highlighted that power quality and voltage stability issues are crucial for expanding the transformation to renewable energy in the power system [6]. The active power flow is intensified and transferred through the clogged transmission system by mitigating the reactive power flow. Equivalently, the rise in reactive power generation at the specific generator influences active power generation.

The Artificial Bee Colony (ABC) [7] and Moth Flame Optimization (MFO) algorithms [8] are nature-inspired heuristic optimization algorithms. The ABC algorithm is based on the foraging behavior of honeybees. This algorithm evolved from analyzing the nature of honeybees searching for food sources; this process of searching for food is called the nectar and is from the ideology of sharing the availability of food sources with other honeybees. The MFO algorithm developed from moths drawing attention to a light source. Moths are commonly attracted to light and adapt their flying directions depending on light intensity. The model of the algorithm is based on the motion of moths and the diminishment of light intensity to explore the optimal intensity of light repetitively. The MFO solves complex optimization problems and holds the finest solution out of all possible solutions.

Furthermore, reactive power is crucial (i) for active power flow in the power system network and (ii) for sustaining the voltage delivering active power in the power system network. For static and dynamic conditions of voltage control, the FACTS devices are efficient in distribution and transmission systems. Their predominant operation is to inject reactive power into the network, which improves the voltage profile of the system.

FACTS devices govern the desired power flow in a system, determine the desirable voltage profile, and reduce transmission losses. Generally, the FACTS devices perform analyses to intensify the power system stability and quality enhancement. FACTS devices perform separately or in collaboration with other FACTS devices, aiming to determine the crucial transmission system parameter activities for favorable grid operation. FACTS devices are classified depending on consequent characteristics, merits, and demerits [9]. FACTS devices, like the Static VAR Compensator (SVC), Thyristor-Controlled Series Capacitors (TCSCs), Static Synchronous Compensators (STATCOMs), Static Synchronous Series Compensators (SSSCs), and Unified Power Flow Controllers (UPFCs), enhance the power quality and voltage stability of the grid.

FACTS devices are peculiar and rapidly interface with power system networks. FACTS devices enhance the power system network to the desired power needed; the UPFC controller comprises two converters and transformers, which are in series with the system and parallel to the system. The UPFC regulates the system's active and reactive power flow separately by injecting the voltage into the transmission line [10–12].

The fundamental intention of the FACTS device is to reduce the power losses in a power grid; thus, most articles about these devices discuss these effects. Numerous researchers have analyzed and proven the benefits of the performance of the UPFC. After all, the optimal placement of the UPFC is essential because of its higher price. Various approaches comprising heuristic, classical, and mixed algorithms are feasible in the literature for determining optimizing issues of FACTSs. Despite the advancements of these methods, there are disadvantages. Heuristic algorithms like Genetic Algorithms, Differential Evolution, Particle Swarm Optimization, and Evolutionary Programming usually perform optimization for problems. These algorithms evaluate the optimum outcome with minimal complications [13].

The optimal power flow (OPF) was identified with a new hybrid decomposition-based multi-objective evolutionary algorithm [14], considering solar and wind integration uncertainties. In the OPF, renewable energy source costs are included to reduce the expenses such that the stability effects of frequency and irregularities of sustainable energy evaluate in the view of operation and cost. Monte Carlo Simulations determine an algorithm's efficiency for all feasible conditions of renewable energy. In [15], the authors suggested a new approach for optimal scheduling problems, including the consequences of irregularities in solar, wind, and loading conditions. The Two-Point Estimate optimization technique and the Genetic Algorithm were employed and simulated on IEEE 30 and 300 bus systems. The results illustrate that the proposed optimal scheduling strategy is effective while testing with GA and TPEM algorithms. In [16], a simulation was performed for a wind–solar Hybrid DC microgrid and the DC fault analysis and power flow was analyzed. The stability of the DC microgrid was analyzed by connecting hybrid sources and performed with distinct DC faults like DC line-to-ground and DC line-to-line faults. The results showed that the system had better load distribution and was barely affected by faults. The voltage did not reach the expected maximum voltage during the fault operation; the maximum power point tracker boosted the hybrid system's performance.

In [17], the authors presented the voltage stability issues of the wind and solar source integrated with a standard IEEE 14 bus system. A modern analytical technique was illustrated to analyze voltage stability. Considering dynamic and PV analyses, a comparative study for performing the system integrated with PV and wind to analyze the voltage stability and determine the desired reactive power for stability enhancement. When PV and wind are integrated with the power grid, the study is examined by the consequence of static analysis with AC contingency and QV curves. The results showed that the PV system infiltration was moderate compared to the wind generation. Thus, the bus voltage variation restricts to a contingency period. The grid voltage stability with infiltration of wind energy was analyzed in [18] with the effects of DFIG-based wind energy and performed under normal and contingency conditions. The optimal location of the shunt FACTS device at the most critical bus significantly enhanced the maximum loadability limit. The SVCs on

bus 5 illustrate the considerable increase in maximum loading factor, λ_{\max} under different cases. In [19], the authors proposed stochastic programming that efficiently integrates renewable energy into the network and examines the optimal sizing, placement, and operating hours for renewable energy sources minimizing the losses. Predefined locations of renewable energy sources are worthy of specifying that energy sources confine to the easy mathematical calculation of planning. A sensitive analysis was executed to identify the effects of planning parameters. Monte Carlo simulation governed the uncertainties, and the modified PSO algorithm solved the proposed stochastic programming modeled as a nonlinear mixed integer stochastic programming. The results showed the improvement in network operation with a better bus voltage profile.

Transient stability enhancement in a hybrid solar–wind-integrated IEEE-14 bus system consolidated with a STATCOM was analyzed in [20]. Under different operating conditions, the respective steady-state analysis was performed to determine the apt sequence of variable solar irradiation and wind speed for reliable operation. The unsymmetrical and symmetrical faults at various locations were conducted with reactive and active power at the point of common coupling (PCC) with and without a STATCOM for examining the voltage analysis. Power fluctuations were smoothed by series compensation. The results showed that the STATCOM can compensate the reactive power with better voltage stability. A reliable evaluation of renewable energy integrating the distribution system analyzed the Electrical Loss Minimization [21] for determining the optimal sizing of DG and the ELM by a Constriction Factor Particle Swarm Optimization (CF-PSO). The RA of EDS obtained the optimal location and sizing of renewable energy and further improved the bus voltages. The results showed the enhanced performance of the integrated system and loss minimization with a better voltage profile comparing the system without distributed generators.

The standard IEEE-30 bus system is considered for integrating wind–solar energy sources for the analysis. Buses 13 and 23 are replaced with a wind generator, and bus 22 is replaced with solar source. The PI controller parameters were fine-tuned using the Marine Predator Algorithm, a recent metaheuristic algorithm, and used with UPFC.

The definite improvement of this article outline is as follows:

- The MPA optimization algorithm optimizes the PI controller gain;
- The proposed MPA–PI-controlled UPFC performance is analyzed on a modified IEEE-30 bus system;
- The MPA optimization algorithm is compared with ABC and MFO.

2. Problem Formulation

The significant motive of the proposed methodology was to reduce active power loss with a sustainable bus voltage of wind-solar integrated power system. It aimed to, moreover, identify the optimal location and size of the system's control variables (UPFC). Consequently, the system model is as follows.

2.1. Reducing Transmission Loss

The minimized transmission line loss of the system determined by Equation (1):

$$E_1 = P^{loss} = \sum_{i=1}^n G_{ij} \left[V_i^2 + V_j^2 - 2V_i V_j \cos(\delta_i - \delta_j) \right] \quad (1)$$

Here, n : number of transmission lines; G_{ij} : Conductance from i^{th} to j^{th} bus; V_i : i^{th} bus voltage; V_j : j^{th} bus voltage; δ_i : Phase angle of the i^{th} bus's voltage; δ_j : Phase angle of the j^{th} bus's voltage; P^{loss} : Transmission active power loss

Transmission loss can minimize using the optimal control variables defined by a vector Y .

$$Y = \left[V_g^1, \dots, V_g^p, Q_{sh}^1, \dots, Q_{sh}^k, tap_n^1, \dots, tap_n^t \right] \quad (2)$$

Here, V_g^p : voltage of a control bus, $i = 1, 2, \dots, p$, Q_{sh}^i : shunt capacitor, i is variable value $1, 2, \dots, k$ and k : total number of shunt capacitors, tap is the total number of transformer tap changer.

$$F = [P_s^1, V_l^1, \dots, V_l^n, Q_g^1, \dots, Q_g^m] \quad (3)$$

Here, P_s^1 : slack bus power, V_l^i : i^{th} bus voltage of load, i is a variable $1, 2, \dots, n$, Q_g^i : i^{th} generator reactive power output, i is variable $1, 2, \dots, m$, and m : total number of generator bus. The primary motive is to reduce power loss and enhance the voltage across the buses through the tolerable analysis of optimal control variables of the system, as in Equation (2).

2.2. Enhancing Bus Voltages

It is a significant issue for maintaining the constant bus voltage during the different loading conditions. The objective function of a healthy profile is defined as:

$$E_2 = \sum_{i=1}^n |V_i - V_{specified}| \quad (4)$$

Here, $V_{specified}$ = bus voltage, n = number of buses.

The essential objective was modified by inequality and equality constraints.

2.2.1. Equality Constraints

Equality constraints for the 'n' bus system represent the power flow equation.

$$P_g^i - P_d^i - V_i \sum_{j=1}^n V_j [g_{ij} \cos(\delta_i - \delta_j) + b_{ij} \sin(\delta_i - \delta_j)] = 0 \quad i = 1, 2, \dots, n \quad (5)$$

$$Q_g^i - Q_d^i - V_i \sum_{j=1}^n V_j [g_{ij} \sin(\delta_i - \delta_j) + b_{ij} \cos(\delta_i - \delta_j)] = 0 \quad i = 1, 2, \dots, n \quad (6)$$

Here, n : number of buses; P_g^i : i^{th} bus generated active power; Q_g^i : i^{th} bus generated reactive power; P_d^i : i^{th} bus demanded active power; Q_d^i : i^{th} bus demanded reactive power; g_{ij} : Conductance from i^{th} to j^{th} bus; b_{ij} : Susceptance from i^{th} to j^{th} bus.

2.2.2. Inequality Constraints

Inequality constraints represent the voltage, active, and reactive power of generator constraints and are defined as:

$$V_{gk}^{min} \leq V_{gk} \leq V_{gk}^{max}, \quad k = 1, 2, 3, \dots, n \quad (7)$$

$$P_{gk}^{min} \leq P_{gk} \leq P_{gk}^{max}, \quad k = 1, 2, 3, \dots, n \quad (8)$$

$$Q_{gk}^{min} \leq Q_{gk} \leq Q_{gk}^{max}, \quad k = 1, 2, 3, \dots, n \quad (9)$$

The constraints of transformer tap setting confine with limited limits.

$$tap_k^{min} \leq tap_k \leq tap_k^{max}, \quad k = 1, 2, 3, \dots, n \quad (10)$$

The reactive power constraints of UPFC confine with limited limits:

$$Q_{min}^{UPFC} \leq Q^{UPFC} \leq Q_{max}^{UPFC} \quad (11)$$

3. Mathematical Modelling of System

The voltage stability of the system essentially relies on voltage magnitude, phase angle, and active power, which are, moreover, sustained by regulating system parameters. Marine

Predator Algorithm (MPA), a recent metaheuristic optimization algorithm, determines the optimal placement of UPFC and PI controller optimal parameters.

3.1. Modeling of Unified Power Flow Controller

Unified Power Flow Controller proposed by L. Gyugyi [22]. The performance of UPFC simultaneously regulates the active, reactive power flow, voltage magnitude, phase angle, and transmission line impedance [23–26]. UPFC, illustrated in Figure 1, includes two voltage-source converters; one is in series with the line, and another interface with a shunt connection [27,28]. The series converter of UPFC achieves its primary function through the series-connected coupling transformer, which supplies the regulated magnitude and phase angle of AC voltage in series with the transmission line. Then, the shunt converter’s primary function is to supply or consume the active power required by the series converter at a common DC link [29]. The electrical model of UPFC is represented in Figure 2.

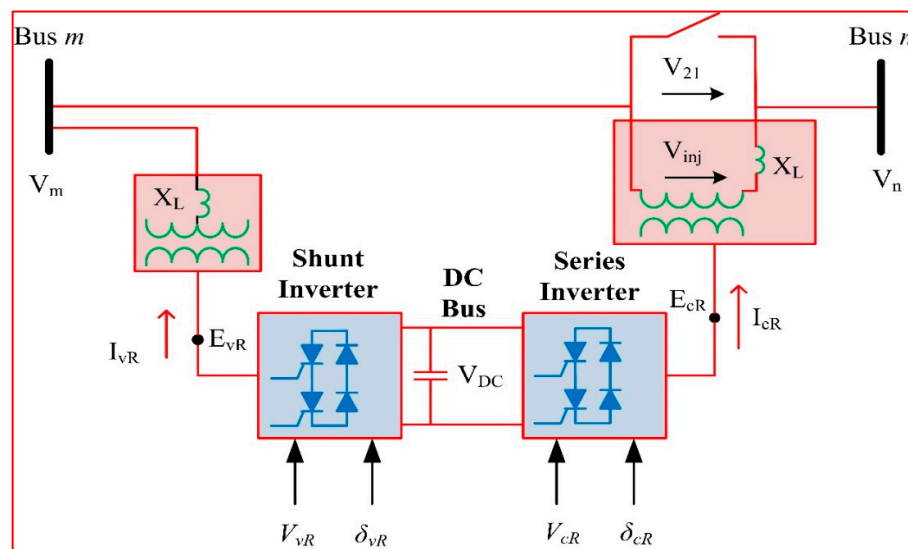


Figure 1. The fundamental design of UPFC.

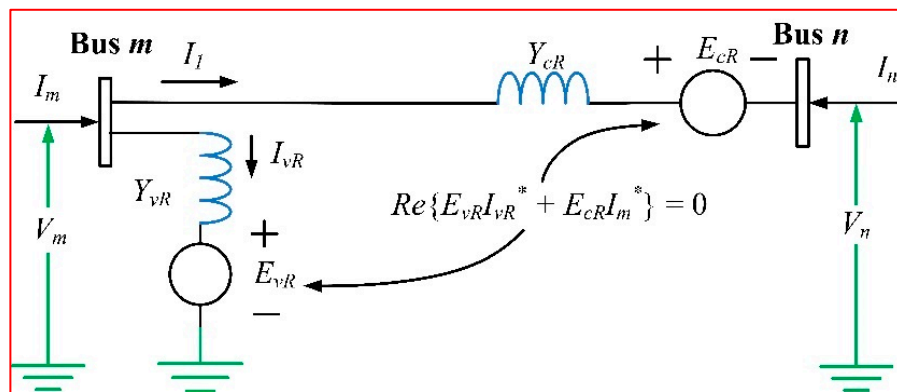


Figure 2. The electrical model of UPFC.

The MPA optimization technique evaluates the optimal placement and PI controller parameters for the performance of the UPFC controller. The inputs of UPFC are PI controller parameters and the optimal location of UPFC power flow analysis on a modified IEEE-30 bus system. As a result, Equations (12)–(25) consider implementing the MPA algorithm.

$$E_{vR} = V_{vR}(\cos\delta_{vR} + j\sin\delta_{vR}) \tag{12}$$

$$E_{cR} = V_{cR}(\cos\delta_{cR} + j\sin\delta_{cR}) \tag{13}$$

$$\operatorname{Re}\left\{-E_{vR}I_{vR}^* + E_{cR}I_m^*\right\} = 0 \quad (14)$$

$$\begin{bmatrix} I_m \\ I_n \end{bmatrix} = \begin{bmatrix} (Y_{cR} + Y_{vR}) & -Y_{cR} & -Y_{cR} - Y_{vR} \\ -Y_{cR} & Y_{cR} & Y_{cR} & 0 \end{bmatrix} \begin{bmatrix} V_m \\ V_n \\ E_{cR} \\ E_{vR} \end{bmatrix} \quad (15)$$

Here: E_{vR} , E_{cR} : voltage sources of UPFC;

V_{vR} : the shunt converter's governable voltage magnitude ($(V_{vR} \min) \leq V_{vR} \leq (V_{vR} \max)$); δ_{vR} : the shunt converter's phase angle ($0 \leq \delta_{vR} \leq 2\pi$); V_{cR} : the series converter's governable voltage magnitude ($(V_{cR} \min) \leq V_{cR} \leq (V_{cR} \max)$); δ_{cR} : the series converter's phase angle ($0 \leq \delta_{cR} \leq 2\pi$) [30].

Bus m :

$$P_m = V_m^2 G_{mm} + V_m V_n [G_{mn} \cos(\theta_m - \theta_n) + B_{mn} \sin(\theta_m - \theta_n)] + V_m V_{cR} [G_{mn} \cos(\theta_m - \delta_{cR}) + B_{mn} \sin(\theta_m - \delta_{cR})] + V_m V_{vR} [G_{vR} \cos(\theta_m - \delta_{vR}) + B_{vR} \sin(\theta_m - \delta_{vR})] \quad (16)$$

$$Q_m = -V_m^2 B_{mm} + V_m V_n [G_{mn} \sin(\theta_m - \theta_n) + B_{mn} \cos(\theta_m - \theta_n)] + V_m V_{cR} [G_{mn} \sin(\theta_m - \delta_{cR}) + B_{mn} \cos(\theta_m - \delta_{cR})] + V_m V_{vR} [G_{vR} \sin(\theta_m - \delta_{vR}) + B_{vR} \cos(\theta_m - \delta_{vR})] \quad (17)$$

Bus n :

$$P_n = V_n^2 G_{nn} + V_n V_m [G_{nm} \cos(\theta_n - \theta_m) + B_{nm} \sin(\theta_n - \theta_m)] + V_n V_{cR} [G_{nn} \cos(\theta_n - \delta_{cR}) + B_{nn} \sin(\theta_n - \delta_{cR})] \quad (18)$$

$$Q_n = -V_n^2 B_{nn} + V_n V_m [G_{nm} \sin(\theta_n - \theta_m) + B_{nm} \cos(\theta_n - \theta_m)] + V_n V_{cR} [G_{nn} \sin(\theta_n - \delta_{cR}) + B_{nn} \cos(\theta_n - \delta_{cR})] \quad (19)$$

Here, P_m , P_n : active power of bus m and bus n ; Q_m , Q_n : reactive power of bus m and bus n ; V_m , V_n = Voltage magnitudes of bus m and bus n , respectively; B_{mm} , B_{nn} = substances between connecting buses m & n ; G_{mn} , G_{nm} = Conductance between buses m & n , respectively; B_{mm} , B_{nn} = substance of bus m and bus n , respectively; G_{mm} , G_{nn} = Conductance at bus m and n , respectively.

Series Converter

$$P_{cR} = V_{cR}^2 G_{nn} + V_{cR} V_m [G_{mn} \cos(\delta_{cR} - \theta_m) + B_{mn} \sin(\delta_{cR} - \theta_m)] + V_{cR} V_n [G_{nn} \cos(\delta_{cR} - \theta_n) + B_{nn} \sin(\delta_{cR} - \theta_n)] \quad (20)$$

$$Q_{cR} = -V_{cR}^2 B_{nn} + V_{cR} V_m [G_{mn} \sin(\delta_{cR} - \theta_m) - B_{mn} \cos(\delta_{cR} - \theta_m)] + V_{cR} V_n [G_{nn} \sin(\delta_{cR} - \theta_n) - B_{nn} \cos(\delta_{cR} - \theta_n)] \quad (21)$$

Shunt Converter

$$P_{vR} = -V_{vR}^2 G_{vR} + V_{vR} V_m [G_{vR} \cos(\delta_{vR} - \theta_m) + B_{vR} \sin(\delta_{vR} - \theta_m)] \quad (22)$$

$$Q_{vR} = V_{vR}^2 B_{vR} + V_{vR} V_m [G_{vR} \sin(\delta_{vR} - \theta_m) - B_{vR} \cos(\delta_{vR} - \theta_m)] \quad (23)$$

$$\Delta P_{bb} = P_{vR} + P_{cR} = 0 \quad (24)$$

$$P_{vR} + P_{cR} = P_m + P_n = 0 \quad (25)$$

where P_{cR} , P_{vR} : Series, and shunt converter active power, respectively; Q_{cR} , Q_{vR} : Series and Shunt converters reactive power, respectively; ΔP_{bb} : power mismatch.

3.2. Proportional–Integral Controller

The advancement in evaluating the controller parameters of proportional and integral gain for shunt and series converters must prefer to enhance the controlled stability [31]. To attain the systems finest outputs, the parameters are adjusted by tuning the control loop. The PI controller is represented in Figure 3. Here, K_p : proportional gain; K_i : integral gain; V_{se} : series converter voltage magnitude; V_{sh} : shunt converter voltage magnitude.

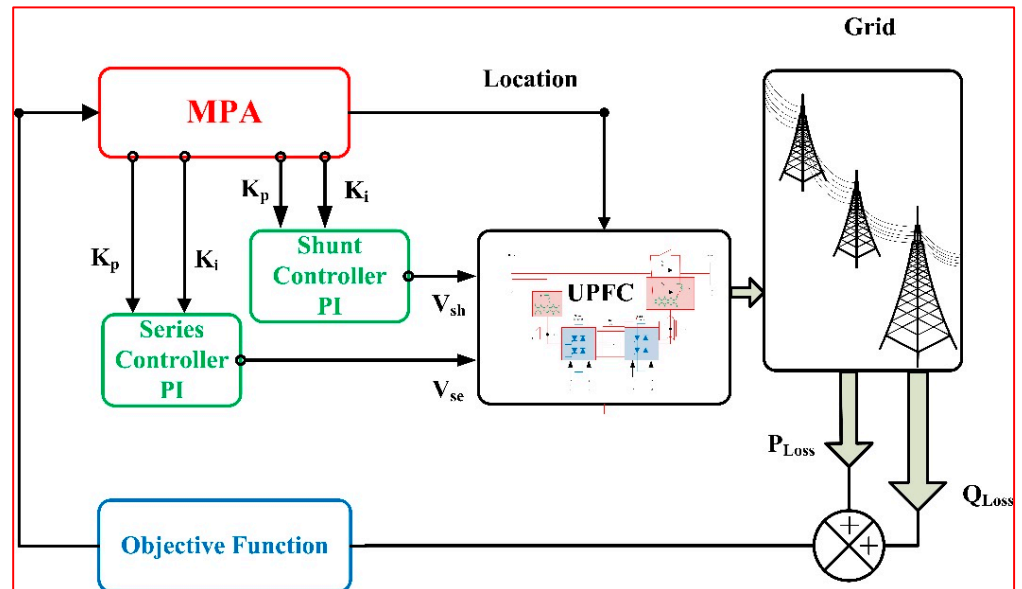


Figure 3. MPA-optimization-based PI controller feed to UPFC.

The MPA algorithm searches for five parameters for each particle, K_p and K_i controller parameters of shunt and series converters, and UPFC optimal location. The Newton–Raphson method evaluates the total power losses of every grid molecule with UPFC.

3.3. Marine Predator Algorithm (MPA)

The Marine Predator Algorithm is an advanced optimization algorithm that draws inspiration from ocean predator evolution when hunting for prey. The searching agents in MPA are the predator and prey, as the predators hunt for prey, consequently searching for its food [32]. Relying upon the possibilities of food while hunting for prey, the marine predators swap between Levy and Brownian strategies. Meanwhile, the food for predators is deficient, and then they approach Levy’s strategy. If the food for predatory is plenty, they approach the Brownian strategy [33]. Levy’s strategy usually involves small steps and exceptionally giant steps. This typical nature can utilize for upgrading searchability in optimization techniques that present effective operation when examined in contrast to reliable random search. As Levy’s approach is efficient, they intensely search neighborhoods because of the small step size; moreover, they search further areas of the domain because of the long step size; they cannot search all areas of the domain alone. However, the Brownian strategy with fixed steps can discover and accomplish the neighboring areas. Consequently, the MPA optimization has a peculiar characteristic nature with these strategies, which is more advantageous; moreover, by combining these strategies accordingly, the domain is perhaps exploited and explored globally and locally.

The MPA optimization algorithm is scattered into three phases considering the ratio of different velocities when reproducing the entire circle of the life of predator and prey. For some iterations, MPA optimization utilizes a pair of Brownian strategies (phase 1 and a half population of phase 2). For other iterations, MPA utilizes the Levy strategy (phase 3 and the remaining half population of phase 2) and, thus, includes both advantages.

However, combining and accurately using individual strategies can specify an organized explorer–exploiter structure that can perform more effectively than the individual strategy. The principal phases of MPA optimization perhaps specified as shown:

A. Initialization

During the initialization process, the variable random positions in the prey and elite matrix include the location vector along the finest adequacy function induced recurring.

B. Phase 1

This phase occurs in the first third of iterations that is defined by $v \geq 10$ (higher-velocity ratio) for excellent investigation capability as the action of prey is quicker than predator [29]. At this instant, the suitable predators reside in stagnation, while the motion of prey is rapid for protecting their food. This stage is expressed mathematically by Equations (26) and (27).

While $Iter < \frac{1}{3}Iter_{max}$

$$\vec{S}_i = \vec{R}_B \otimes \left(\vec{Elite}_i - \left(\vec{R}_B \otimes \vec{Prey}_i \right) \right) \quad i = 1, 2, \dots, n \quad (26)$$

$$\vec{Prey}_i = \vec{Prey}_i + \left(0.5\vec{R} \otimes \vec{S}_i \right) \quad (27)$$

Here, \vec{S}_i : the size of the predator step, \vec{R}_B : a random number vector depending on a standard distribution of Brownian motions, \vec{R} : a uniform random variable [0, 1], and n is the number of searching agents per population.

C. Phase 2

This phase course arises at the second-third of iterations, while the exploration tries to transform transiently to exploitation. This phase expresses as $v \approx 1$ (unity velocity ratio); hence, the motion of predator and prey is in the same step.

While $\frac{1}{3}Iter_{max} < Iter < \frac{2}{3}Iter_{max}$. Depending on Levy's strategy, Equations (28) and (29) determine the first half of the population.

$$\vec{S}_i = \vec{R}_L \otimes \left(\vec{Elite}_i - \left(\vec{R}_L \otimes \vec{Prey}_i \right) \right) \quad i = 1, 2, \dots, n/2 \quad (28)$$

$$\vec{Prey}_i = \vec{Prey}_i + \left(0.5\vec{R} \otimes \vec{S}_i \right) \quad (29)$$

Random number vector (R_L) that depends on a standard distribution of the Levy motions. Furthermore, the Brownian approach upgrades the second half of the population by Equations (30) and (31).

$$\vec{S}_i = \vec{R}_B \otimes \left(\left(\vec{R}_B \otimes \vec{Prey}_i \right) - \vec{Prey}_i \right) \quad i = n/2, \dots, n \quad (30)$$

$$\vec{Prey}_i = \vec{Elite}_i + \left(0.5X_f \otimes \vec{S}_i \right) \quad (31)$$

Here, variable X_f governs the predator's step size and is mathematically expressed as Equation (32).

$$X_f = [1 - (Iter/Iter_{max})]^{(2 \times Iter/Iter_{max})} \quad (32)$$

D. Phase 3

This phase is dedicated to the last third of iterations, which is mainly related to higher exploitation ability. This phase expresses a lower velocity ratio ($v = 0.1$); hence, the motion of

the predator is quicker than the prey. Depending on the Levy movement, the mathematical representation of this phase is as Equations (33) and (34).

While $Iter > \frac{2}{3}Iter_{max}$,

$$\vec{S}_i = \vec{R}_L \otimes \left(\left(\vec{R}_L \otimes \vec{Elite}_i \right) - \vec{Prey}_i \right) \quad i = 1, 2, \dots, n \quad (33)$$

$$\vec{Prey}_i = \vec{Elite}_i + \left(0.5X_f \otimes \vec{S}_i \right) \quad (34)$$

E. Finishing

After each iteration, the elite matrix updates the best feasible solution; the last iteration is the final solution. Figure 4 illustrates the significant steps of the MPA-optimization algorithm.

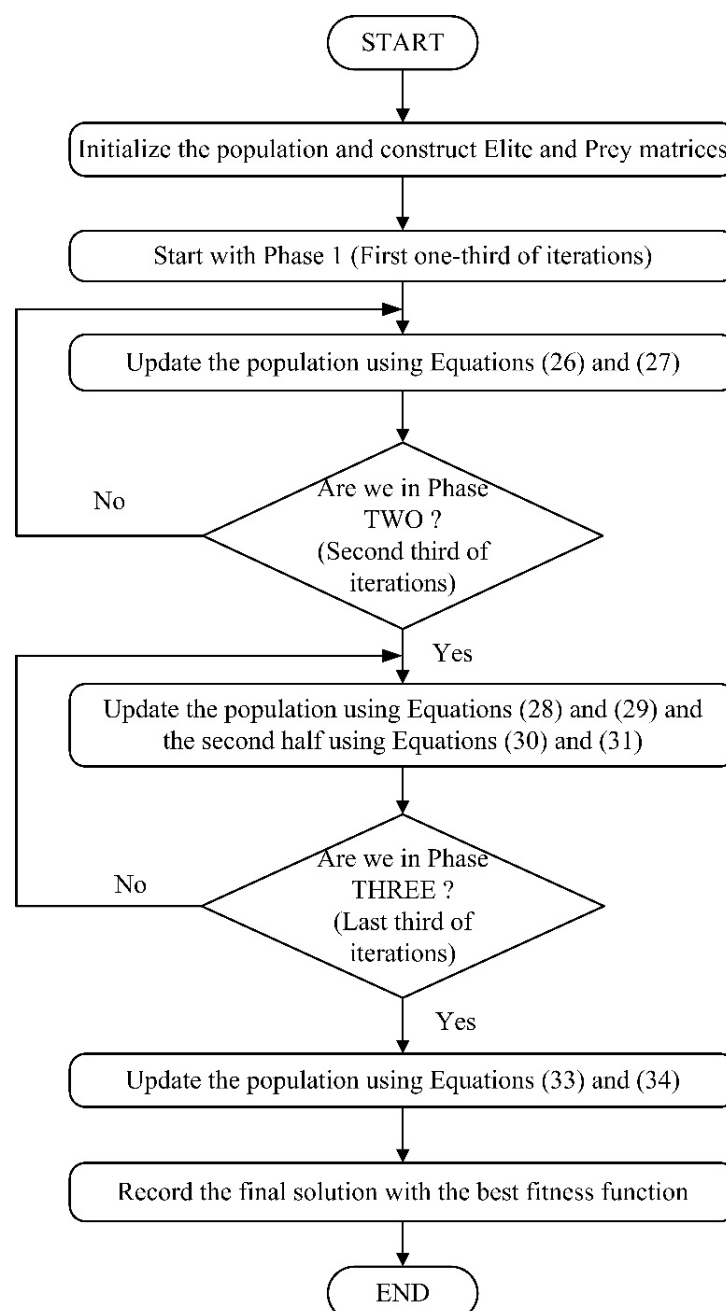


Figure 4. Flowchart of the MPA-optimization technique.

Furthermore, the MPA optimization algorithm robustness and effectiveness analysis on 23 classical test functions was compared with two potent optimization algorithms: Artificial Bee Colony and Moth-Flame Optimization. For balance testing, three algorithms were performed with a uniform parameter set-up: the population size was 30, and maximum iterations were 100. These 23 classical test functions were considered for the analysis of the MPA and determined the efficacy of optimization algorithms. From classical test functions, the first seven test functions (TF1-TF7) were categorized as unimodal, whereas the test functions (TF8-TF23) were multimodal. Categorically, the unimodal test function analyzed the exploitation response, whereas the multimodal test function analyzed the exploration response of the optimization algorithm.

3.4. Modeling of Wind and Solar Power

Wind and solar power sources integrate with the transmission network, and detailed modeling of the wind farm and the solar farms are as follows.

A. Wind Power Model

Various investigations focused on obtaining desirable data on wind speed considering the special distributions. Amongst those, the efficiently authenticated model was the Weibull probability density function [34,35], which is capable of actual wind speed distribution because its adaptability is feasible and soothes operation. DFIG-WECS [36] could generate and absorb the reactive power and coordinate the terminal voltage of the bus—accordingly, the DFIG-WECS stator integrated into the transmission system, as the rotor connected to the transmission system through a variable converter. The wind speed distribution represented by the Weibull probability density function as:

$$F_v(v) = \frac{k}{\lambda} \left(\frac{v}{\lambda}\right)^{(k-1)} e^{-\left(\frac{v}{\lambda}\right)^k}, v > 0 \quad (35)$$

Here, v : wind speed; λ and k : scale and shape parameters, respectively. The values of these parameters were considered from [33]. At bus 13, the wind generator parameters k and λ values are 2 and 9, respectively. At bus 23, the wind generator parameters k and λ values are 2 and 10, respectively.

The results in [37] state that the load demand was achieved by two wind and one solar power source. Accordingly, we considered two wind power sources. One wind source at bus 13 is the combined power of 25 turbines, and another at bus 23 is the combined power of 20 turbines.

The overall wind source-rated output power is 3 MW and the mathematical derivation of the actual output power associated with wind speed defines this as:

$$P_w(v) = \begin{cases} 0, & v < v_{in} \text{ or } v > v_{out} \\ P_{wr} \left(\frac{v-v_{in}}{v_r-v_{in}}\right), & v_{in} \leq v \leq v_r \\ P_{wr}, & v_r < v \leq v_{out} \end{cases} \quad (36)$$

Here, P_{wr} : wind turbines rated output power; cut in and cut out wind speeds $v_{in} = 3$ m/s, $v_{out} = 25$ m/s; rated wind speed $v_r = 16$ m/s.

B. Solar Power Model

A solar PV generator replaced the thermal generator at bus 22. Solar irradiance is the only primary source for solar power generation. The irradiance data were excluded because of the unavailability of solar irradiance data and the varying seasons. From [37,38], the solar irradiance is expressed by the Lognormal probability density function as:

$$F_G(G) = \frac{1}{G\sigma\sqrt{2\pi}} e^{-\frac{(\ln G - \mu)^2}{2\sigma^2}}, G > 0 \quad (37)$$

Here, G is solar irradiance. $\mu = 6$ and $\sigma = 0.6$ are the mean and standard deviation. Solar PV depending on solar irradiance is expressed as:

$$P_S(G) = \begin{cases} P_{sr} \left(\frac{G^2}{G_s G_c} \right), & 0 < G < G_c \\ P_{sr} \left(\frac{G}{G_s} \right), & G \geq G_c \end{cases} \quad (38)$$

Here, P_{sr} : Solar output power of 50 MW; the solar irradiance at the conventional environment and a particular irradiance point is $G_s = 800 \text{ W/m}^2$ and $G_c = 120 \text{ W/m}^2$, respectively.

4. Results and Discussion

The performance analysis of the proposed MPA-PI optimization for reducing active power loss and improving the voltage profile under varying load conditions was simulated on a modified IEEE 30 bus transmission system by MATLAB coding. The transmission system comprised six generators at buses 1, 2, 13, 22, 23, and 27. Out of six generators, two were wind farm generators, one was a solar PV generator, and the remaining three were thermal generators. The total active power demand was 238.40 MW, and the reactive power demand was 126.20 MVAR. The optimal location of UPFC was connected to buses 12–15. Figure 5 shows a modified IEEE-30 bus system and the MPA optimization algorithm with UPFC performed on it. The MPA optimization algorithm was executed in MATLAB programming language. The actual power losses evaluated considering the UPFC device for different loading conditions like 100%, 110%, and 120% of base loading.

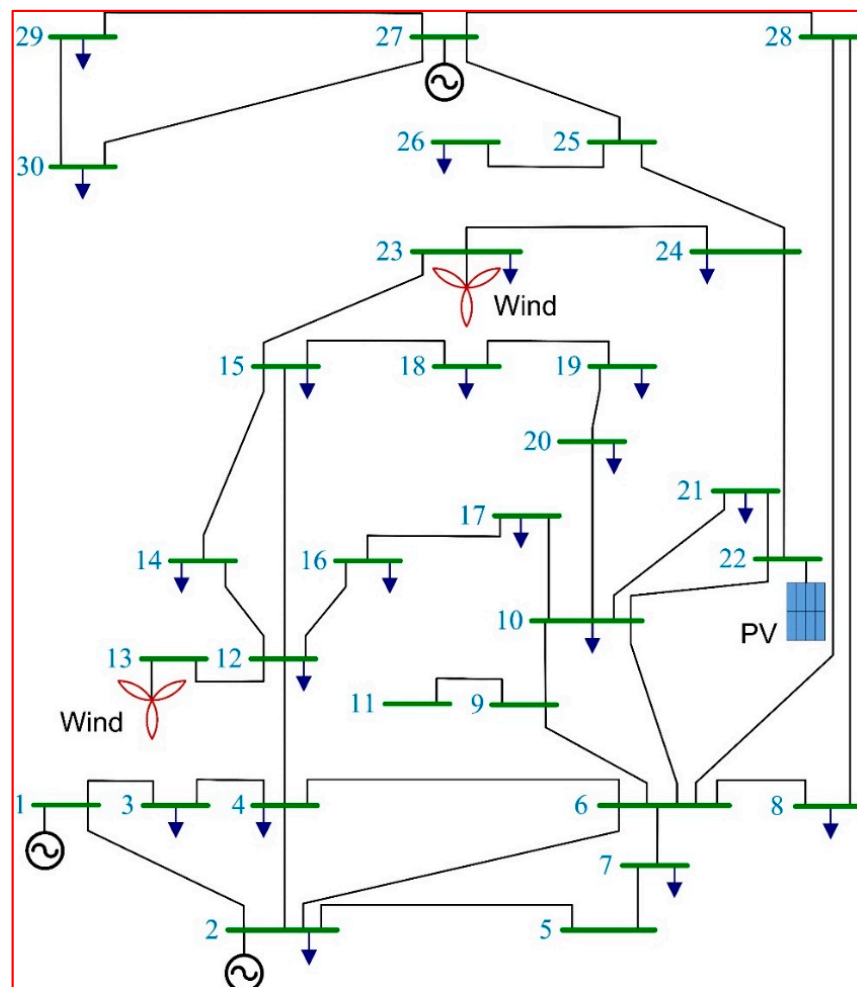


Figure 5. Integrated Wind, PV with modified IEEE 30 System.

The minimum power loss and optimal voltage was evaluated with and without UPFC. The MPA optimization evaluated the system performance in four cases to determine the system's active power loss and voltage magnitude. The first case was without the UPFC device, and the remaining three cases were with the UPFC device and varying base load conditions by 10%. The bus voltage magnitudes of 30 buses were determined and tabulated in Table 1. The minimized loss was evaluated after connecting the UPFC device; the voltage values were determined from the N-R method, and evaluated voltage with the proposed method with 100% base load condition without UPFC and with UPFC device are compared and plotted in Figure 6. For 110% base load, the voltage profile without and with UPFC is represented in Figure 7. For 120% base load, the voltage profile without and with UPFC represent in Figure 8.

Table 1. Voltage profile (p.u.) without and with UPFC under different base load conditions.

Bus Number	100% of Base Load		110% of Base Load		120% of Base Load	
	Without UPFC	With UPFC	Without UPFC	With UPFC	Without UPFC	With UPFC
1	1.04	1.04	1.04	1.04	1.04	1.04
2	1.023	1.023	1.003	1.003	0.993	0.994
3	0.9748	0.97	0.9666	0.9673	0.9626	0.9628
4	0.977	0.9821	0.9675	0.9698	0.9659	0.9732
5	0.9702	0.9702	0.9622	0.9622	0.9667	0.9669
6	0.9824	0.9973	0.9733	0.9745	0.9627	0.9638
7	0.973	0.9783	0.9691	0.971	0.9613	0.9646
8	1.002	1.002	0.9803	0.9803	0.9803	0.9803
9	1.0013	1.0098	1.0223	1.0239	1.0169	1.0194
10	0.9624	0.9791	0.9963	0.9985	0.9855	0.9876
11	1.053	1.053	1.041	1.042	1.041	1.041
12	0.9489	0.9565	0.9787	0.9904	0.9871	0.9903
13	1.052	1.052	1.052	1.054	1.042	1.042
14	0.954	0.9681	0.9832	0.9958	0.9874	0.9893
15	0.9441	0.9523	0.9761	0.9789	0.9832	0.9914
16	0.9533	0.9687	0.9859	0.9887	0.9842	0.9891
17	0.9602	0.9753	0.9987	1.0043	0.997	1.0004
18	0.9391	0.9501	0.9619	0.9659	0.9655	0.9745
19	0.9465	0.9523	0.9712	0.9795	0.9989	1.0012
20	0.9562	0.9613	0.9788	0.9811	0.9885	0.9921
21	0.9561	0.9644	0.9738	0.9812	0.9645	0.9781
22	0.9629	0.9712	0.9833	0.9912	0.9752	0.9825
23	0.9523	0.9632	0.9938	1.005	0.9765	0.9858
24	0.9647	0.9754	0.9719	0.9845	0.9665	0.9736
25	0.9683	0.9821	0.9723	1.0012	0.967	0.9807
26	0.9597	0.9623	0.9623	1.0056	0.9687	0.9749
27	0.9629	0.9687	0.982	0.9928	0.9749	0.9823
28	0.982	0.9954	0.984	0.9945	0.9774	0.9827
29	0.9667	0.9743	0.9825	0.9964	0.9691	0.9729
30	0.9503	0.9612	0.9678	0.9723	0.9745	0.9859

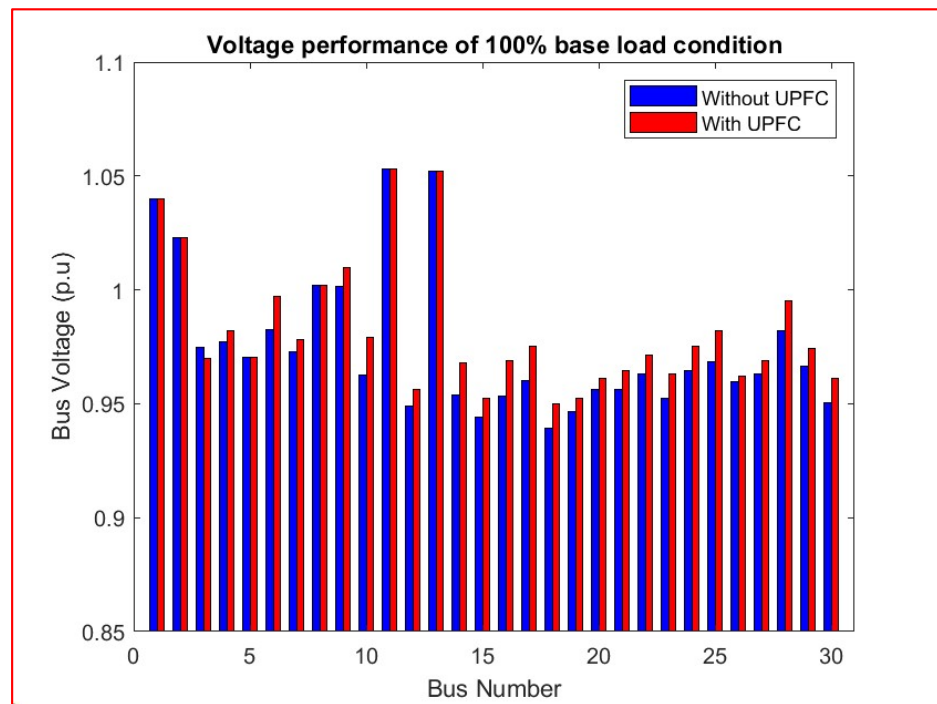


Figure 6. Voltage profile with 100% base load condition.

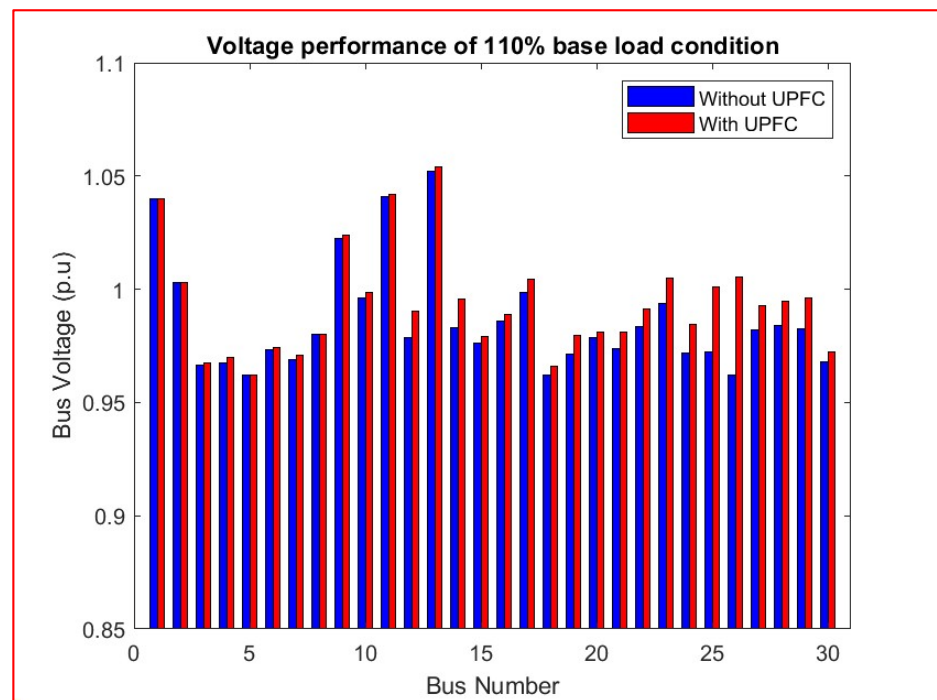


Figure 7. Voltage profile with 110% base load condition.

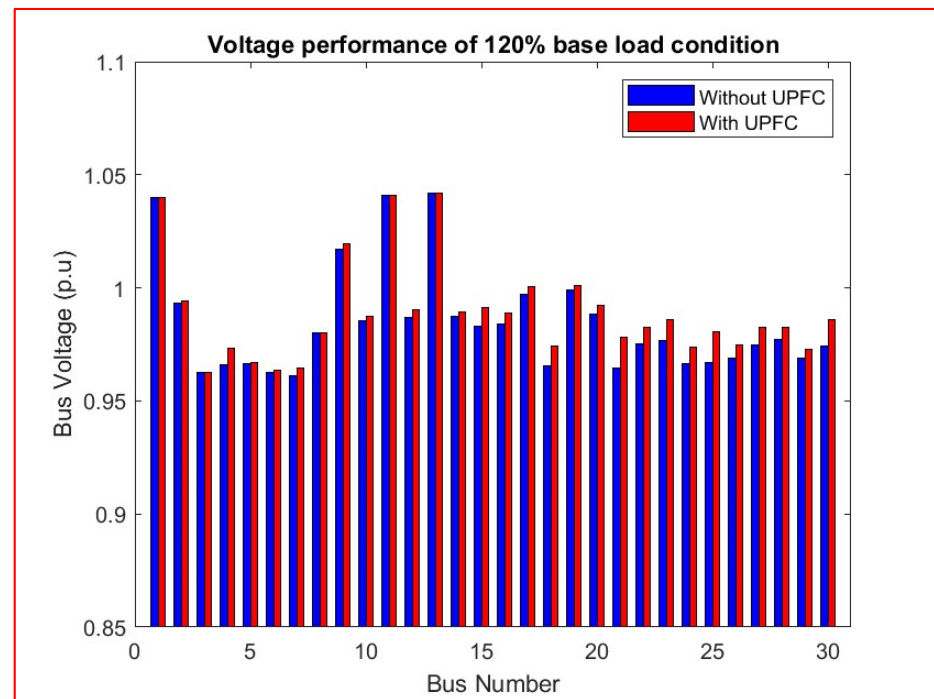


Figure 8. Voltage profile with 120% base load condition.

The gains of a proportional integral controller for UPFC fine-tuned with the MPA optimization algorithm. The power losses are input variables for the MPA optimization, and the PI controller values tabulate in Table 2.

Table 2. Analysis of proportional–integral parameters with proposed optimization.

Proportional–Integral Parameters			
K_{p_s}	K_{i_s}	$K_{p_{sh}}$	$K_{p_{sh}}$
0.018	7.34×10^{-4}	0.0956	0.0323

Significantly, the MPA possessed quick convergence compared to variant optimization algorithms, whereas the MPA effectively converged, favoring optimal value in concise searching operations. Thus, it validates the firmness of MPA by accomplishing the precise equity among exploitation and exploration intelligence. Bonferroni–Dunns test were chosen as the statistical analysis of MPA, which a post hoc statistical analysis. This test illustrates a substantially different performance among the algorithms, whenever dissimilarities in the average ranking were higher than the critical difference. The convergence characteristics of power loss (MW) using MPA at various loads are plotted in Figures 9–11.

Compared with the heuristic algorithms like ABC and MFO optimization algorithms, the active power losses obtained from the MPA optimization algorithm exhibited competitive performance. The comparison results showed a significant improvement in the performance of the system. The active power loss was evaluated based on loss with the UPFC device at different base loadings like 100%, 110%, and 120% of base load. Therefore, it is evident from Table 3 that the optimal position of FACTS devices effectively reduced the system’s active power loss. Moreover, the MPA–PI-optimization algorithm was efficient, when compared to other optimization algorithms, in reducing the active power loss in all congested lines.

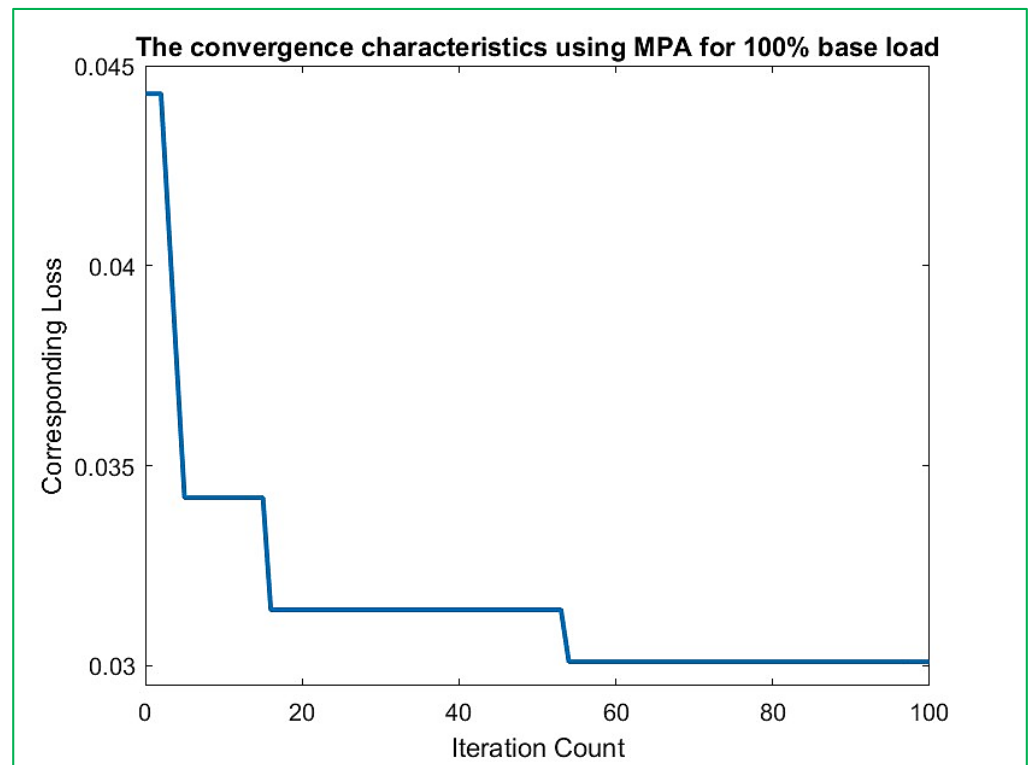


Figure 9. The convergence characteristics of power losses using MPA for 100% base load.

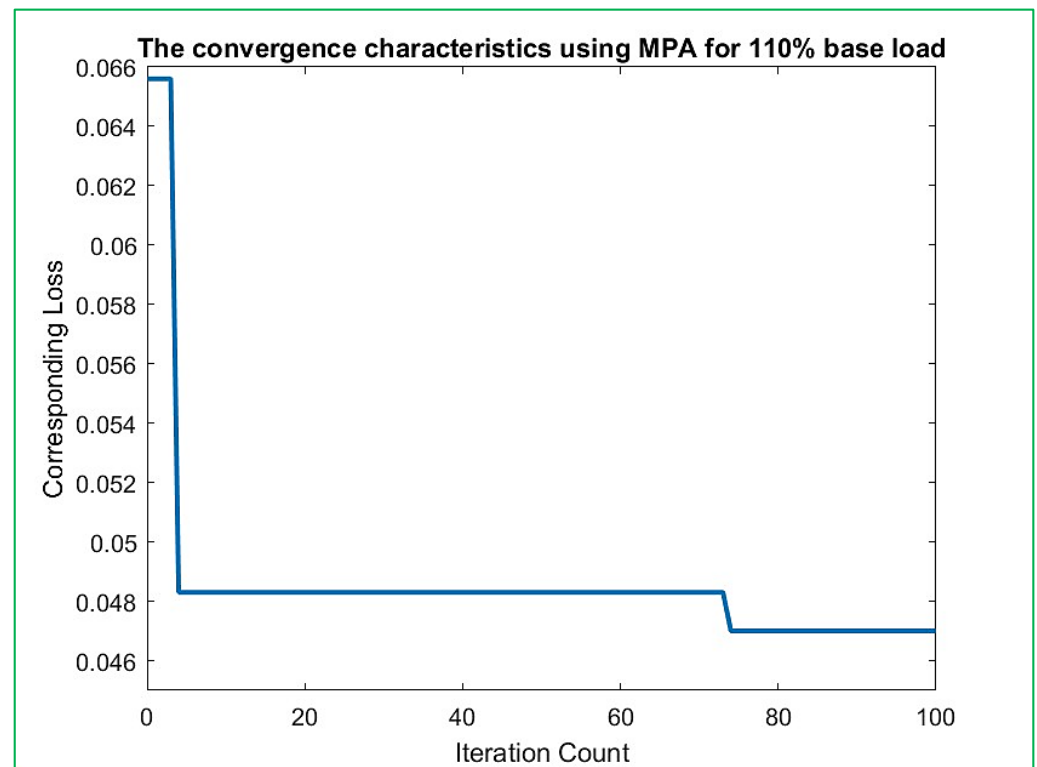


Figure 10. The convergence characteristics of power losses using MPA for 110% base load.

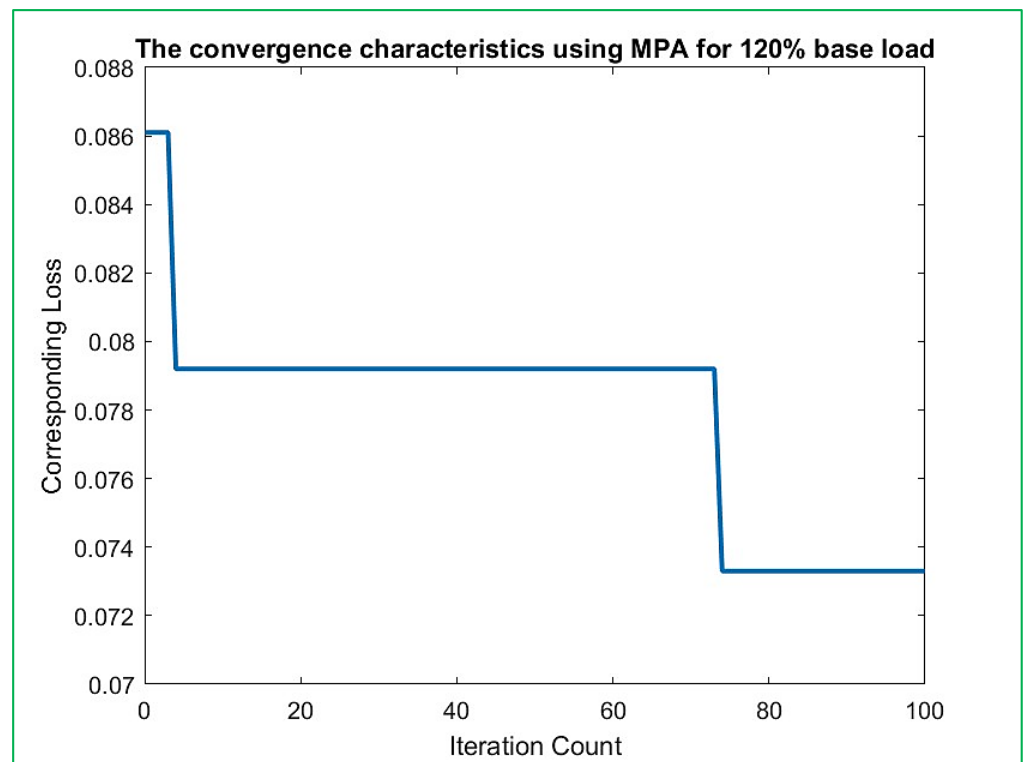


Figure 11. The convergence characteristics of power losses using MPA for 120% base load.

The graph for the percentage of loss reduction for different base loads is plotted in Figure 12. At 100% base load, the loss reduction with MPA was 68.39%, which was better than the ABC and MFO optimization techniques. At 110% base load, the loss reduction of MPA was 74.33%, and at 120% of base load, the loss reduction was 69.89%.

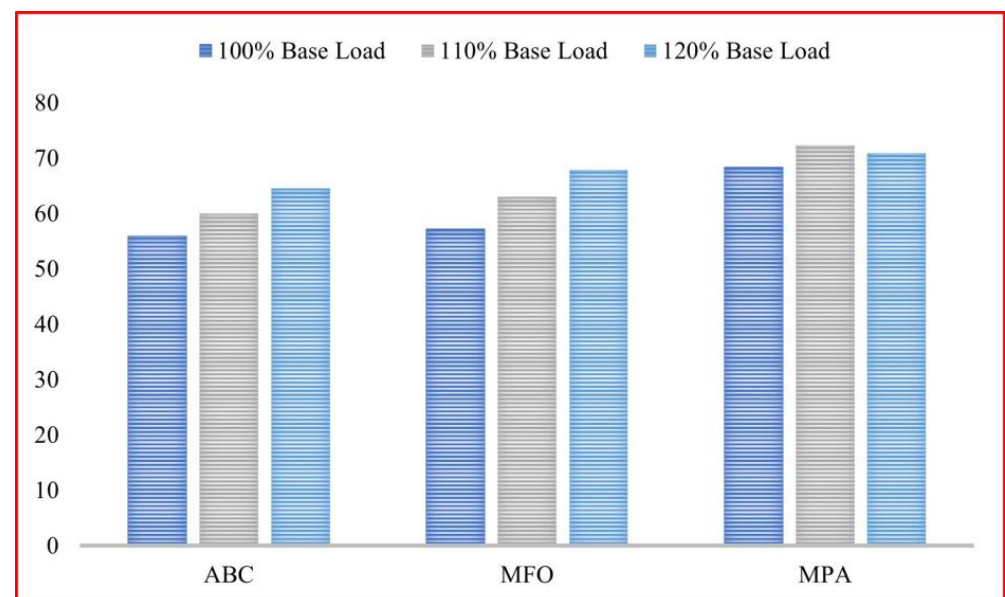


Figure 12. Percentage of loss reduction at different loads using ABC, MFO, and MPA.

Table 3. Analysis of active power loss with and without UPFC.

Loading Pd and Qd (%)	Active Power Loss without UPFC (p.u)	Active Power Loss with UPFC (p.u)	Evolutionary Algorithm with UPFC
100	0.0622	0.0328	ABC
		0.0320	MFO
		0.0301	MPA
110	0.0865	0.0479	ABC
		0.0473	MFO
		0.0470	MPA
120	0.1185	0.0742	ABC
		0.0738	MFO
		0.0733	MPA

5. Conclusions

The performance of a new metaheuristic optimization algorithm-based optimum PI controller for UPFC was discussed in this paper. The proposed MPA optimization algorithm determined the optimal values of PI gain and the optimal placement of UPFC—the proposed algorithm performed on a modified IEEE-30 bus system. The performance efficiently reduced losses—the optimal placement of UPFC connected to bus 12 and bus 15. The analysis used a modified wind–solar-integrated IEEE-30 bus system, considering the corresponding probability density functions for simulating irregularities in renewable energy sources under increasing power system loadability. The results show that the proposed MPA algorithm effectively reduced the active power losses, improved the voltage profile, and satisfied all constraints.

The MPA optimization algorithm may be applicable for the problem of integration of wind and solar system in electric grid and it is possible for expansion for real power and reactive power management in larger power system networks.

Author Contributions: Conceptualization, C.V.; methodology, C.V. and S.C.; software, C.V.; validation, C.V.; formal analysis, C.V.; investigation, C.V.; resources, C.V.; data curation, C.V.; writing—original draft preparation, C.V.; writing—review and editing, S.C.; visualization, S.C.; supervision, S.C. All authors have read and agreed to the published version of the manuscript.

Funding: This research received no external funding.

Data Availability Statement: Not applicable.

Conflicts of Interest: We want to assure you that potential conflicts of interest did not influence our research’s reporting and that we have complied with the journal’s policy on conflicts of interest.

References

- Sharif, A.; Raza, S.A.; Ozturk, I.; Afshan, S. The dynamic relationship of renewable and nonrenewable energy consumption with carbon emission: A global study with the application of heterogeneous panel estimations. *Renew. Energy* **2019**, *133*, 685–691. [\[CrossRef\]](#)
- GWEC. Global Wind Report. 2023. Available online: <https://gwec.net/globalwindreport2023/> (accessed on 11 April 2023).
- Abdel-Basset, M.; Mohamed, R.; Mirjalili, S.; Chakraborty, R.K.; Ryan, M. An Efficient Marine Predators Algorithm for Solving Multi-Objective Optimization Problems: Analysis and Validation. *IEEE Access* **2021**, *9*, 42817–42844. [\[CrossRef\]](#)
- Heard, B.P.; Brook, B.W.; Wigley, T.M.L.; Bradshaw, C.J.A. The Burden of Proof: A comprehensive review of the Feasibility of 100% renewable-electricity systems. *Renew. Sustain. Energy Rev.* **2017**, *76*, 1122–1133. [\[CrossRef\]](#)
- Brown, T.W.; Bischof-Niemz, T.; Blok, K.; Breyer, C.; Lund, H.; Mathiesen, B.V. Response to ‘Burden of proof: A comprehensive review of the Feasibility of 100% renewable electricity systems. *Renew. Sustain. Energy Rev.* **2018**, *92*, 834–847. [\[CrossRef\]](#)
- Tang, Z.; Hill, D.J.; Liu, T. Two-stage voltage control of sub-transmission networks with high penetration of wind power. *Control Eng. Pract.* **2017**, *62*, 1–10. [\[CrossRef\]](#)
- Ettappan, M.; Vimala, V.; Ramesh, S.; Kesavan, V.T. Optimal reactive power dispatch for real power loss minimization and voltage stability enhancement using Artificial Bee Colony Algorithm. *Microprocess. Microsyst.* **2020**, *76*, 103085. [\[CrossRef\]](#)
- Balakumar, S.; Getahun, A.; Kefale, S.; Kumar, K.R. Improvement of the Voltage Profile and Loss Reduction in Distribution Network Using Moth Flame Algorithm: Wolaita Sodo, Ethiopia. *J. Electr. Comput. Eng.* **2021**, *2021*, 9987304. [\[CrossRef\]](#)

9. Siddique, A.; Xu, Y.; Aslam, W.; Rasheed, M. A Comprehensive Study on FACTS Devices to Improve the Stability and Power Flow Capability in Power System. In Proceedings of the 2019 IEEE Asia Power and Energy Engineering Conference (APEEC), Chengdu, China, 29–31 March 2019.
10. Rezaeian-Marjani, S.; Jalalat, S.M.; Tousi, B.; Galvani, S.; Talavat, V. A probabilistic approach for optimal operation of wind-integrated power systems, including UPFC. *IET Renew. Power Gener.* **2023**, *17*, 706–724. [[CrossRef](#)]
11. Zand, M.; Nasab, M.A.; Padmanaban, S.; Maroti, P.K.; Muyeen, S.M. Sensitivity analysis index to determine the optimal location of multi-objective UPFC for improvement of power quality parameters. *Energy Rep.* **2023**, *10*, 431–438. [[CrossRef](#)]
12. Ye, C.; Xu, T.; Wang, T.; Zhang, J.; Xi, P. Research on locating and sizing method of unified power flow controller (UPFC). In Proceedings of the CIRED 2022 Shanghai Workshop, Online Conference, Shanghai, China, 21–22 September 2022.
13. Čalasan, M.; Konjić, T.; Kecejević, K.; Nikitović, L. Optimal allocation of static var compensators in electric power system. *Energies* **2020**, *13*, 3219. [[CrossRef](#)]
14. Avvari, R.K.; D.M., V.K. Multi-Objective Optimal Power Flow including Wind and Solar Generation Uncertainty Using New Hybrid Evolutionary Algorithm with Efficient Constraint Handling Method. *Int. Trans. Electr. Energy Syst.* **2022**, *2022*, 7091937. [[CrossRef](#)]
15. Reddy, S.S. Optimal scheduling of thermal-wind-solar power system with storage. *Renew. Energy* **2017**, *101*, 1357–1368. [[CrossRef](#)]
16. Zulu, M.; Ojo, E. Power Flow and Fault Analysis Simulation for A PV/Wind Hybrid DC Microgrid. In Proceedings of the 30th Southern African Universities Power Engineering Conference (SAUPEC), Durban, South Africa, 25–27 January 2022.
17. Youssef, E.; El Azab, R.M.; Amin, A.M. Comparative study of voltage stability analysis for renewable energy grid-connected systems using PSS/E. In Proceedings of the Southeast Con 2015, Fort Lauderdale, FL, USA, 9–12 April 2015.
18. Adetokun, B.B.; Muriithi, C.M.; Ojo, J.O. Voltage stability assessment and enhancement of power grid with increasing wind energy penetration. *Int. J. Electr. Power Energy Syst.* **2020**, *120*, 105988. [[CrossRef](#)]
19. Hemmati, R.; Ghiasi, S.M.S.; Entezariharsini, A. Power fluctuation smoothing and loss reduction in grid integrated with thermal-wind-solar-storage units. *Energy* **2018**, *152*, 759–769. [[CrossRef](#)]
20. Sengupta, S.; Kumar, A.; Tiwari, S. Transient Stability Enhancement of a Hybrid Wind-PV Farm incorporating a STATCOM. In Proceedings of the 2018 3rd IEEE International Conference on Recent Trends in Electronics, Information & Communication Technology (RTEICT), Bangalore, India, 18–19 May 2018.
21. Kumar, S.; Sarita, K.; Vardhan, A.S.S.; Elavarasan, R.M.; Saket, R.K.; Das, N. Reliability Assessment of Wind-Solar PV Integrated Distribution System Using Electrical Loss Minimization Technique. *Energies* **2020**, *13*, 5631. [[CrossRef](#)]
22. Gyugyi, L. Unified power-flow control concept for flexible AC transmission systems. *IEE Proc. C Gener. Transm. Distrib.* **1992**, *139*, 323–331. [[CrossRef](#)]
23. Suliman, M.Y.; Al-Khayyat, M.T. Power flow control in parallel transmission lines based on UPFC. *Bull. Electr. Eng. Inform.* **2020**, *9*, 1755–1765. [[CrossRef](#)]
24. Sharma, P.; Singh, H. Modeling and Simulation of UPFC to Improve Power Quality. In Proceedings of the 2022 2nd International Conference on Advance Computing and Innovative Technologies in Engineering (ICACITE), Greater Noida, India, 28–29 April 2022.
25. Siva, R.; Reddy, S. Power loss minimization in a transmission system by optimally identifying various FACTS devices using HGAPSO heuristic method. *I-Manag. J. Future Eng. Technol.* **2021**, *16*, 30–37.
26. Rezaeian-Marjani, S.; Nazarpour, D.; Galvani, S. Data clustering-based probabilistic UPFC allocation for improving power system reliability considering correlated uncertain variables. *Int. Trans. Electr. Energy Syst.* **2021**, *31*, 13153. [[CrossRef](#)]
27. Ahmad, A.A.; Sirjani, R. Optimal placement and sizing of multi-type FACTS devices in power systems using metaheuristic optimization techniques: An updated review. *Ain Shams Eng. J.* **2020**, *11*, 611–628. [[CrossRef](#)]
28. Waghade, S.N.; Gowder, C. Modeling and Simulation of Voltage Source Model of UPFC in an IEEE 9 Bus System for Power Flow Enhancement. *Int. J. Eng. Res. Technol.* **2020**, *9*, 75–80.
29. Sita, H.; Reddy, P.U.; Kiranmayi, R. Optimal location and sizing of UPFC for optimal power flow in a deregulated power system using a hybrid algorithm. *Int. J. Ambient. Energy* **2020**, *43*, 1413–1419. [[CrossRef](#)]
30. AL-Rubayi, R.H.; Ibrahim, L.G. Enhancement transient stability of power system using UPFC with M-PSO. *Indones. J. Electr. Eng. Comput. Sci.* **2020**, *17*, 61–69. [[CrossRef](#)]
31. Amin, I.; Mahmood, D.; Numan, A. Optimal localization of UPFC for transmission line losses minimizing using particle swarm optimization. *Eng. Technol. J.* **2021**, *39*, 1463–1472. [[CrossRef](#)]
32. Faramarzi, A.; Heidarinejad, M.; Mirjalili, S.; Gandomi, A.H. Marine Predators Algorithm: A nature-inspired metaheuristic. *Expert Syst. Appl.* **2020**, *152*, 113377. [[CrossRef](#)]
33. Houssein, E.H.; Gad, A.G.; Hussain, K.; Suganthan, P.N. Major advances in particle swarm optimization: Theory, analysis, and application. *Swarm Evol. Comput.* **2021**, *63*, 100868. [[CrossRef](#)]
34. Souza, R.R.; Balbo, A.R.; Martins, A.C.; Soler, E.M.; Baptista, E.C.; Sousa, D.N.; Nepomuceno, L. A Gradient-Based Approach for Solving the Stochastic Optimal Power Flow Problem with Wind Power Generation. *Electr. Power Syst. Res.* **2022**, *209*, 108038. [[CrossRef](#)]
35. Tavakoli, A.; Karimi, A. Development of Monte-Carlo-based stochastic scenarios to improve uncertainty modeling for optimal energy management of a renewable energy hub. *IET Renew. Power Gener.* **2023**, *17*, 1139–1164. [[CrossRef](#)]

36. Eladl, A.A.; Basha, M.I.; ElDesouky, A.A. Techno-economic multi-objective reactive power planning in integrated wind power system with improving voltage stability. *Electr. Power Syst. Res.* **2023**, *214*, 108917. [[CrossRef](#)]
37. Biswas, P.P.; Suganthan, P.N.; Amaratunga, G.A.J. Optimal power flow solutions incorporating stochastic wind and solar power. *Energy Convers. Manag.* **2017**, *148*, 1194–1207.
38. Avvari, R.K.; DM, V.K. A new hybrid evolutionary algorithm for multi-objective optimal power flow in an integrated WE, PV, and PEV power system. *Electr. Power Syst. Res.* **2023**, *214*, 108870. [[CrossRef](#)]

Disclaimer/Publisher’s Note: The statements, opinions and data contained in all publications are solely those of the individual author(s) and contributor(s) and not of MDPI and/or the editor(s). MDPI and/or the editor(s) disclaim responsibility for any injury to people or property resulting from any ideas, methods, instructions or products referred to in the content.